A Microphysical Connection Among Biomass Burning, Cumulus Clouds, and Stratospheric Moisture

Steven Sherwood

Science **295**, 1272 (2002);
DOI: 10.1126/science.1065080

are much smaller, but a preliminary analysis of a larger data set suggests that this result is not representative (*18*). There is a discrepancy between the anisotropy factors (i.e., the τ_{max}/τ_{min} ratios): The fast-moving (*19, 20*) Australian plate has a small anisotropy factor of 2.7, whereas the slow-moving North European plate exhibits maximum anisotropy factors of 35 to 100 under Fennoscandia. This result is surprising, because geodynamic models suggest that the greater the strain imparted on the mantle by an overriding tectonic plate, the greater the expected degree of alignment of olivine crystals in the direction of plate motion. Therefore, a greater degree of alignment should be expected below the Australian plate than below the Fennoscandian plate if electrical anisotropy is linked to present-day plate motion. In both target areas, the high-conductance directions coincide with seismic fast directions (*7, 9*). We suggest that the anisotropy detected in the mantle below the Fennoscandian plate is either a relic of paleoflow in the mantle, induced at a time when the mantle in this region was subjected to a larger strain, or is indicative of sublithospheric convection dominating mantle flow (*16*). If the alignment is preserved over geological time scales, this would imply that the relaxation time of the mantle is more than 10^7 years and longer than hitherto believed, providing a useful constraint on geodynamic models for convective flow (*21*) and the evolution of lattice-preferred orientation in olivine aggregates.

References and Notes

1. J.-P. Montagner, T. Tanimoto, *J. Geophys. Res.* **96**, 20337 (1991).
2. M. Mareschal *et al.*, *Nature* **375**, 134 (1995).
3. K. Bahr, A. Duba, *Earth Planet. Sci. Lett.* **178**, 87 (2000).
4. F. Simpson, *Nature* **412**, 632 (2001).
5. S. J. Mackwell, D. L. Kohlstedt, *J. Geophys. Res.* **95**, 5079 (1990).
6. S.-I. Karato, *Nature* **347**, 272 (1990).
7. E. Debayle, B. L. N. Kennett, *J. Geophys. Res.* **105**, 25423 (2000).
8. The confidence intervals of the electromagnetic strike angle are estimated by applying the error propagation law to the formula that links the strike angle to the elements of the magnetotelluric impedance tensor (*4*).
9. L. P. Vinnik, L. I. Makeyeva, A. Milev, A. Yu. Usenko, *Geophys. J. Int.* **111**, 433 (1992).
10. K. Bahr, M. Bantin, Chr. Jantos, E. Schneider, W. Storz, *Phys. Earth Planet. Inter.* **119**, 237 (2000).
11. U. Schmucker, *Phys. Earth Planet. Inter.* **7**, 365 (1973).
12. I. L. Osipova, S. E. Hjelt, L. L. Vanyan, *Phys. Earth Planet. Inter.* **53**, 337 (1989).
13. Y. Xu, T.-J. Shankland, B. T. Poe, *J. Geophys. Res.* **105**, 27865 (2000).
14. P. Suhadolc, G. F. Panza, St. Mueller, *Tectonophysics* **176**, 123 (1990).
15. F. Simpson, *J. Geophys. Res.* **105**, 19321 (2000).
16. H. Schmeling, G. Marquart, *Phys. Earth Planet. Inter.* **79**, 241 (1993).
17. For a three-layer model consisting of a resistive lithosphere of thickness h, a conductive sublithospheric layer of conductance τ, and a moderately resistive (100 ohm · m) upper mantle in which the electromagnetic field at an angular frequency ω has a penetration depth p, both the real (Re) and imaginary (Im) parts of the Schmucker-Weidelt transfer function $C(\omega)$ at this frequency are polynomials in $\omega\mu_0\tau p$ (*10*), where μ_0 is free space permeability. For conductances τ that are so large that $\omega\mu_0\tau p \gg 1$, the magnetotelluric phase ϕ is linked to the model parameters by

$$\tan(\phi) = -\frac{\mathrm{Re}\, C}{\mathrm{Im}\, C} = \omega\mu_0\tau h$$

Here, h is estimated after solving the static shift problem of magnetotellurics (e.g., by extension to long periods) or by a comparison to a reference model. If h is known, then τ can be computed from ϕ for periods short enough to ensure that $\omega\mu_0\tau h \gg 1$ but long enough to ensure that Re $C > h$ (*10*). If the second condition is violated, then the resulting conductance is a lower bound of the actual conductance.
18. A. Gatzemeier, personal communication.
19. A. E. Gripp, R. G. Gordon, *Geophys. Res. Lett.* **17**, 1109 (1990).
20. S. Wang, R. Wang, *Earth Planet. Sci. Lett.* **189**, 133 (2001).
21. É. Kaminski, N. M. Ribe, *Earth Planet. Sci. Lett.* **189**, 253 (2001).

22. Data acquisition with the German long-period magnetotelluric cluster in Scandinavia was made possible by the German Science Foundation under contract Ba 889/8 and an internal grant from Geoforschungszentrum Potsdam. We thank F. Echternacht, M. Engels, E. Eggert-Heise, T. Korja, J. Leibecker, K. Roden, and E. Steveling for organizing the field campaign.

10 September 2001; accepted 7 January 2002

A Microphysical Connection Among Biomass Burning, Cumulus Clouds, and Stratospheric Moisture

Steven Sherwood

A likely causal chain is established here that connects humidity in the stratosphere, relative humidity near the tropical tropopause, ice crystal size in towering cumulus clouds, and aerosols associated with tropical biomass burning. The connections are revealed in satellite-observed fluctuations of each quantity on monthly to yearly time scales. More aerosols lead to smaller ice crystals and more water vapor entering the stratosphere. The connections are consistent with physical reasoning, probably hold on longer time scales, and may help to explain why stratospheric water vapor appears to have been increasing for the past five decades.

Data collected during the last half-century appear to indicate an approximate doubling of stratospheric water vapor during this period, of which approximately half can be accounted for by increases in stratospheric production of water vapor by methane oxidation (*1*). The other half presumably results from increases in the moisture content of air entering the stratosphere through the tropical tropopause. However, temperatures near this entry point, which were thought to regulate stratospheric moisture levels, have not increased during recent decades (*2, 3*). This implies that either relative humidity near the tropopause has substantially increased, or other pathways exist whereby moisture can enter the stratosphere. The importance of this problem is underscored by recent findings that stratospheric moisture increases may be a significant contributor to global temperature trends (*4*) and may also interfere with the recovery of polar ozone by exacerbating destruction mechanisms (*5*).

I show that fluctuations in stratospheric humidity can indeed be caused by fluctuations in relative humidity just below the tropical tropopause, which in turn are governed by the sizes of ice crystals lofted in deep convective updrafts. The moisture content of air entering the stratosphere is thought to be controlled by condensation of vapor to the ice phase in transient lifting events outside of convective cells and/or phase changes within intense convective cells themselves (*6*). The relative importance of these two controlling factors is unknown. Convective moistening or drying should depend not only on temperature but also on the propensity of lofted ice to evaporate at a level high enough (>14 to 15 km) so that the vapor will enter the stratosphere rather than subsiding back into the troposphere (*7, 8*). It has been widely assumed that condensation outside of convection resets the water vapor to a lower value independent of convective influence, but the evidence presented here argues against this assumption.

This study uses data acquired from 1992 to 1998. Ice crystal "effective diameter" D_e was retrieved near the tops of deep cumulonimbus clouds (Cb) using the ISCCP (International Satellite Cloud Climatology Project) B3 archive of radiance observations by the AVHRR (Advanced Very High Resolution Radiometer) on

Department of Geology and Geophysics, Yale University, New Haven, CT 06520, USA. E-mail: steven.sherwood@yale.edu

board the NOAA (National Oceanic and Atmospheric Administration) polar orbiter series (*9, 10*). Cb were defined as clouds whose 11-μm brightness temperatures were less than 210 K, indicating tops in the region above 14 km where the air is slowly rising toward the stratosphere (*6*). Water vapor observations came from HALOE (Halogen Occultation Experiment) (*11*); available vertical profiles from each month were interpolated to surfaces of constant potential temperature θ and averaged over a tropical belt. Temperature fields near the tropical tropopause were obtained by applying a specially designed analysis method to radiosonde temperature data at 100 hPa (*12*). On the time and space scales considered here, temperature anomalies at 100 hPa are expected to be representative of those at other levels near the tropopause (*13, 14*).

The large (~5 to 10 K peak-to-peak) annual cycles in tropopause temperature, T, and saturation water vapor mixing ratio with respect to ice, q_s (a function of T), cause a corresponding annual cycle in water vapor mixing ratio, q, of similar size and phase to that of q_s (*15, 16*). Because changes in q not caused by temperature are sought, however, the relative humidity q/q_s is considered. Strict thermodynamic control of water vapor would imply constant relative humidity. Because vapor concentrations can relax toward thermodynamic equilibrium only where condensed phases are present, the tropical $\langle q_s(t)\rangle$ was computed here using a weighted mean with horizontal weighting proportional to the observed monthly mean 100-hPa frequency of cloud occurrence (*17*). An unweighted computation was also performed for comparison.

The results of this analysis are summarized in Fig. 1 (*18*). The quantity $RH^*_\theta(t)$ used to show humidity is defined as $q[\theta, + \delta t_\theta/\langle q_s(t)\rangle]$, where q is the mean mixing ratio observed by HALOE within a tropical belt (here, 20°S to 20°N) at the target level θ, and δt_θ is the time required for air to rise from just below the tropopause (370 K) to θ (*19*). Thus, RH* gives the ratio of an air layer's eventual humidity (after it has slowly lofted to θ) to its initial saturation humidity at time t when the layer is just below the tropopause. The precise mean value of RH* is not very meaningful because it depends on the vertical weighting of the HALOE retrieval and the exact vertical matching of the temperature and moisture data. The important feature in Fig. 1 is RH fluctuations of ~30%, which occur on a variety of time scales, notably semiannual.

It takes several months or longer for air to rise the ~4 km from the 370 K level to the 450 K level. During this time, q at a given height often changes substantially. Nonetheless, RH* fluctuations are remarkably similar at the two levels. This "tape recorder" effect (*16*) is well known for seasonal thermodynamic changes but reappears here more generally. The 450 K level is above all significant dehydration. Moisture variations reaching this level enter what is known as the "tropical pipe" region (*20*) where they must ultimately affect the entire stratosphere. Dehydration or mixing on the way from 370 K to 450 K removed about 30% of the moisture regardless of the initial value, preserving moisture variations below the tropopause rather than erasing or clipping them.

Fluctuations of the observed mean effective diameter D_e of Cb ice crystals are also tightly correlated with those of RH* at both levels (Fig. 1). The correlations are highly significant regardless of the range of latitudes used in computing q or $\langle q_s\rangle$ (Table 1), strongly supporting a physical connection between D_e and RH. This is also true if Cb weighting of the temperature field is not implemented, although the correlation drops significantly (*21*); this result supports the contention that only temperatures in the presence of clouds affect ambient vapor amounts.

The significance of the correlations, together with the lack of any common instrument between the observations of D_e and those of RH, enables us to reject the possibility of accidental association due to instrument sampling or accuracy issues (*22*). The only worry is if some atmospheric constituent happens to be contaminating both the ISCCP and HALOE retrievals in a similar, systematic manner. The only likely contaminants would be aerosols near the tropopause or stratospheric moisture itself (*23*). Aerosol is measured by the CLAES (Cryogenic Limb Array Etalon Spectrometer) instrument flying together with HALOE (*24*); examination of CLAES aerosol time series (*25*) showed essentially zero correlation with the traces in Fig. 1, ruling out aerosols as a spurious source of correlation. Radiative effects of stratospheric moisture cannot account for the magnitude or sign of the correlation (*23*). Thus, we cannot explain the data other than by accepting the D_e-RH relationship as physical.

Two straightforward interpretations of this relationship are possible. First, smaller ice crystals may increase RH; second, higher RH may reduce crystal size. These possibilities may be distinguished observationally: Any influence of RH on D_e would have to operate locally and would cause instantaneous spatial covariability of the two quantities as a result of the short lifetimes (~1 hour) of Cb, whereas influences of D_e on RH (thus q) would not appear locally because of the long lifetime (≫1 day at these altitudes) over which q variations can spread out horizontally. The data show that the global relationship does not exist locally (Fig. 2), ruling out the second interpretation. Before accepting that D_e controls RH, however, we must ensure that the observed sensitivity is physically reasonable.

Observations of cumulus clouds indicate a distribution of particle sizes that usually drops off steeply below 10 μm and above 30 to 40 μm, with varying proportions within this range and occasional bimodality (*26*). The simplest way of treating this situation is to assume the presence of two size modes, taken here to be $D_1 = 10$ μm and $D_2 = 30$ μm. The populations of these two modes may be affected by variations in the number of particles nucleated at lower levels. In the deepest Cb, however, the total water content (ND^3, where N is the number of crystals) of rising parcels should be unaffected by such

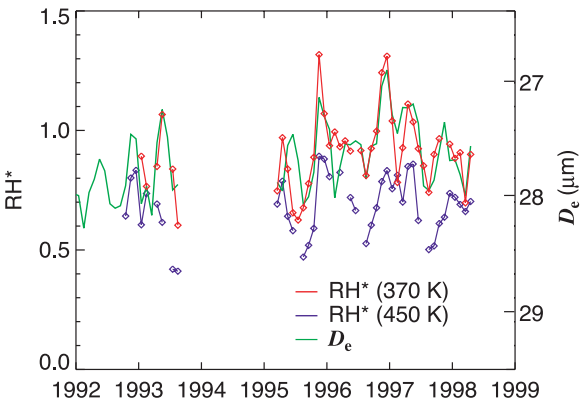

Fig. 1. Effective ice radius D_e in Cb clouds and observed RH^*_θ (plotted versus 370 K crossing time) at θ = 370 K and θ = 450 K (see text for definition). Gap in observations is due to excessive orbit decay of NOAA-11. Scale for D_e at right decreases toward the top. Measures of statistical association are given in Table 1.

Table 1. Linear correlation coefficients r between monthly tropical means of RH* and D_e, with P values for each correlation. The P value indicates the probability that the observed correlation could have occurred by chance, assuming 20 degrees of freedom in the data (*36*). The standard case refers to RH^*_{370} computed using HALOE data from 20°N to 20°S, with Cb weighting of q_s as described in the text. Also listed are results at 450 K, results using HALOE data within different latitude limits, and results obtained without Cb weighting of q_s (i.e., with uniform weighting). The standard and 450 K cases are those graphed in Fig. 1.

Conditions	r	P
Standard case	0.70	0.0003
450 K level	0.62	0.0020
HALOE (10°N to 10°S)	0.66	0.0008
HALOE (25°N to 25°S)	0.70	0.0003
q_s unweighted	0.53	0.0012

influences because it is strongly regulated in Cb by cloud-dynamical factors. This assumption implies

$$\delta N_1 \sim -27\delta N_2 \quad (1)$$

for microphysical variations.

Smaller ice crystals should evaporate much more rapidly than larger ones and should settle more slowly, thus leaving vapor closer to the tropopause. If we treat the crystals as ice spheres, then Stokes flow applies at these sizes and their terminal fall speed scales as D^2. Sublimation for these sizes is governed primarily by diffusion with only minor effects due to ventilation (*27*), so it will be approximately proportional to surface area ND^2. Therefore, the amount of vapor q' sublimated into a thin layer near the top of the outflow by a unit mass of ice scales simply as

$$q' \sim N = N_1 + N_2 \quad (2)$$

If we consider an increase $\varepsilon = \delta N_1/N$ in the proportion of small particles, then Eqs. 1 and 2 imply an increase in sublimation rate of $\delta q'/q' = 0.96\varepsilon$. To relate variations of the source q' to those of the ambient amount q, it is reasonable to assume that $q = aq'$, where a is a constant (*28*). The effective diameter

$$D_e = \frac{N_1 D_1^3 + N_2 D_2^3}{N_1 D_1^2 + N_2 D_2^2} \quad (3)$$

decreases for positive ε by an amount that depends on the population ratio N_1/N_2. For $N_1 = N_2$, D_e changes from 28 μm to (28 – 3.7ε) μm.

Putting these results together, we obtain an estimated 26% increase in q per 1.0-μm decrease in D_e (independent of a). This estimate is well within a factor of 2 of the empirical ratio in Fig. 1. The estimate can be altered by roughly a factor of 2, either by changing the mode population ratio by a factor of 10 or by changing the size distribution to a very wide or unimodal one. Although our calculation is a crude one, it shows that the interpretation of Fig. 1 as control of q by D_e is physically reasonable.

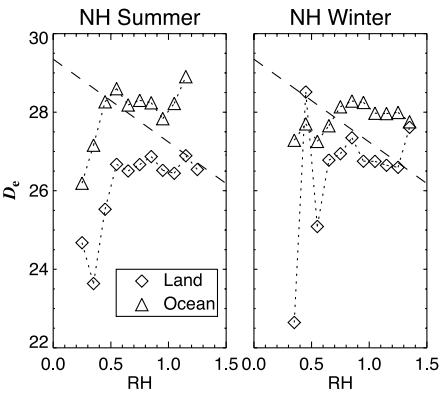

Fig. 2. Mean D_e versus RH. Plotted points were obtained by binning all retrievals in 1-month × 5° latitude × 10° longitude boxes and averaging boxes by RH^*_{370}. Land results include only boxes that are mostly land; ocean results include only boxes that are mostly ocean. The dashed lines show the regression slope from the comparison in Fig. 1.

Can this effect explain the observed increases in stratospheric moisture over time? For this to be so, mean D_e would have to show a decrease of ~1 μm over the past 50 years. Unfortunately, trends in tropical-mean D_e cannot be verified using AVHRR at this time because of the lack of an adequate absolute solar reflectivity calibration. However, indirect evidence for them does exist.

Aerosols are capable of nucleating new droplets in cumulus clouds, giving them the potential to increase ice particle numbers and reduce their sizes (*29*). A recent examination of D_e in Cb (*9*) found that spatial and temporal variations in D_e on interannual and longer time scales were closely associated with variations in smoke and/or dust generated in biomass burning regions. The semiannual variation of D_e in Fig. 1 is in phase with the semiannual variation in biomass burning, which occurs predominantly in the spring of both hemispheres. A variety of regional trends in D_e, apparently due to aerosol, were found in different continental regions and spanned a range of ~1.5 μm/decade. The trends lack absolute calibration, but if only a small majority of them were toward smaller D_e (more aerosol), their overall average could easily match the –0.2 μm/decade needed to explain the stratospheric moisture increase.

Estimation of the global mean trend in D_e may be attempted by multiplying its empirical sensitivity to aerosol by the estimated trend in biomass burning. According to one estimate, tropical biomass burning has increased by 50% since the middle of the 19th century, with most of the increase occurring in the last 50 years (*30*). For this to explain the stratospheric moisture trend (assuming linear sensitivity) would require ΔD_e, the reduction in tropical-mean D_e brought about by all present-day burning, to be 2 to 3 μm. This would be moderate compared to observed climatological D_e variations. However, quantifying ΔD_e accurately is very difficult without more extensive aerosol information, because it is impossible to tell what D_e would be in the absence of burning sources, especially over oceans. Half of Cb occur over oceans, and most continental Cb occur after the local burning season, so ΔD_e would definitely fall short of the required 2 to 3 μm unless aerosol sources were currently affecting clouds at considerable distances. However, this may actually be the case if clouds in unpolluted regimes (such as over oceans) are highly susceptible to small inputs of smoke, as suggested by some observations (*31*). Nor is biomass burning the only potential source of aerosol; airborne dust may also have increased as a result of land-use impacts or circulation changes (*32*).

Further studies with more capable instrumentation will be vital to a better understanding of how aerosols and water vapor may be connected by cloud mechanisms. A finely calibrated, long-term record may prove necessary before we can draw more definitive conclusions concerning stratospheric moisture trends.

References and Notes

1. K. H. Rosenlof *et al*., *Geophys. Res. Lett.* **28**, 1195 (2001).
2. D. J. Seidel, R. J. Ross, J. K. Angell, G. C. Reid, *J. Geophys. Res.* **106**, 7857 (2001).
3. X. L. Zhou, M. A. Geller, M. H. Zhang, *J. Geophys. Res.* **106**, 1511 (2001).
4. P. M. D. Forster, K. P. Shine, *Geophys. Res. Lett.* **26**, 3309 (1999).
5. D. B. Kirk-Davidoff, E. J. Hintsa, J. Anderson, D. W. Keith, *Nature* **402**, 399 (1999).
6. S. C. Sherwood, A. E. Dessler, *Geophys. Res. Lett.* **27**, 2513 (2000).
7. H. S. Johnston, S. Solomon, *J. Geophys. Res.* **84**, 3155 (1979).
8. S. C. Sherwood, A. E. Dessler, *J. Atmos. Sci.* **58**, 765 (2001).
9. S. C. Sherwood, *J. Clim.*, in press.
10. The Cb ice crystal size estimates were obtained by empirically decomposing AVHRR 3.7-μm Cb solar reflectances into the product of three terms: one function of viewing geometry, one function of time, and a residual (variance-minimized) term indicating the individual scene reflectance anomaly. The decomposition gives an accurate estimate of variations in effective diameter D_e (the mean ice crystal diameter weighted by surface area) from which orbital and scanning variations have been removed.
11. J. E. Harries *et al*., *J. Geophys. Res.* **101**, 10205 (1996).
12. S. C. Sherwood, *J. Geophys. Res.* **105**, 29489 (2000).
13. J. E. Frederick, A. R. Douglass, *Mon. Weather Rev.* **111**, 1397 (1983).
14. E. J. Highwood, B. J. Hoskins, *Q. J. R. Meteorol. Soc.* **124**, 1579 (1998).
15. E. M. Weinstock, E. J. Hintsa, A. E. Dessler, J. G. Anderson, *Geophys. Res. Lett.* **22**, 3231 (1995).
16. P. W. Mote *et al*., *J. Geophys. Res.* **101**, 3989 (1996).
17. The saturation mixing ratio $q_s(t)$ is first averaged in monthly 5° × 10° longitude-latitude bins, then the bin values for each month are weighted by that month's bin Cb populations (or not, for the unweighted case) and averaged. Condensed water may occur independently of Cb in the form of thin cirrus clouds, but observations indicate that the horizontal distribution of these clouds is similar to that of Cb, so the weighting should be appropriate regardless of which cloud type is most important.
18. A table of the individual monthly data and their sample uncertainties is available on *Science* Online at www.sciencemag.org/cgi/content/full/295/5558/1272/DC1.
19. These lag times were computed from a monthly climatology of radiatively balanced vertical velocities calculated by K. Rosenlof (*16*).
20. R. A. Plumb, *J. Geophys. Res.* **101**, 3957 (1996).
21. The difference between correlation coefficients (0.70 and 0.53) has only a 12% likelihood of being this large by chance, even under the overly conservative assumption that the experiments are completely independent.
22. Errors in D_e and RH* due to poor sampling or random instrumental errors contribute only to the uncorrelated variance and are accounted for in the cited significance figures.
23. Aerosols in the lower stratosphere are known to affect HALOE retrievals. These effects are removed as part of the retrieval algorithm, but removal may not be perfect. Stratospheric moisture slightly absorbs the radiation used to observe D_e, but absorption by higher humidity would lead to larger D_e, the opposite of the observed relationship.

24. S. T. Massie *et al.*, *J. Geophys. Res.* **101**, 9757 (1996).
25. S. Sherwood, data not shown.
26. H. Pruppacher, J. D. Klett, *Microphysics of Clouds and Precipitation* (Kluwer, Dordrecht, Netherlands, ed. 2, 1997).
27. W. Ji, P. K. Wang, *J. Atmos. Sci.* **56**, 829 (1999).
28. The linearity assumption follows by noting from Fig. 1 that there was no apparent lag between variations in D_e and RH, and that the dehydration rate below 450 K was roughly proportional to q. The former circumstance implies a quasi-steady balance between sources and sinks of q near the tropopause, whereas the latter implies that the sinks (thus sources) must be proportional to q.
29. V. T. J. Phillips, T. W. Choularton, A. M. Blyth, J. Latham, *Q. J. R. Meteorol. Soc.*, in press.
30. R. A. Houghton, in *Global Biomass Burning*, J. S. Levine, Ed. (MIT Press, Cambridge, MA, 1991), pp. 321–325.
31. D. Rosenfeld, *Science* **287**, 1793 (2000).
32. C. Moulin, C. E. Lambert, F. Dulac, U. Dayan, *Nature* **387**, 691 (1997).
33. C. S. Bretherton, M. Widmann, V. P. Dymnikov, J. M. Wallace, I. Bladé, *J. Clim.* **12**, 1990 (1999).
34. G. H. Orcutt, S. F. James, *Biometrika* **35**, 397 (1948).
35. M. S. Bartlett, *J. R. Stat. Soc.* **98**, 536 (1935).
36. The number 20 was obtained by visually estimating the number of independent fluctuations in the data and subtracting 1. Computations using two common formulas based on autocovariance models (*33*) valid for general (*34*) and red-noise (*35*) processes yielded 18 and 37 degrees of freedom, respectively. All of these estimates are high enough to yield strongly significant results.
37. I thank A. Dessler for generously supplying key interpolated data sets, K. Rosenlof for providing vertical velocity calculations, A. Heymsfield for useful advice, and H. Zeleznik for editorial assistance. The ISCCP AVHRR data were obtained from the NASA Langley Atmospheric Sciences Data Center. Supported by NASA Earth Observing System Interdisciplinary Science program grant UPN 291-01-91.

6 August 2001; accepted 9 January 2002

Warming of the Southern Ocean Since the 1950s

Sarah T. Gille

Autonomous Lagrangian Circulation Explorer floats recorded temperatures in depths between 700 and 1100 meters in the Southern Ocean throughout the 1990s. These temperature records are systematically warmer than earlier hydrographic temperature measurements from the region, suggesting that mid-depth Southern Ocean temperatures have risen 0.17°C between the 1950s and the 1980s. This warming is faster than that of the global ocean and is concentrated within the Antarctic Circumpolar Current, where temperature rates of change are comparable to Southern Ocean atmospheric temperature increases.

The Southern Ocean plays a critical role in global climate. With no continental barriers, it serves as a conduit to transmit climatic signals between the Pacific, Atlantic, and Indian Oceans. The predominant current of the Southern Ocean, the fast-flowing Antarctic Circumpolar Current (ACC), is characterized by strongly tilting isopycnals. Because water mixes preferentially along constant density surfaces, tilting isopycnals bring mid-depth water into contact with the ocean surface and serve as a barrier to southward transport, possibly helping to isolate the Antarctic continent from mid-latitude climate variability (*1*).

Recent examinations of global ocean temperature changes have shown substantial warming in the upper 1000 m, averaging about 0.1°C between 1955 and 1995 (*2*). Southern Hemisphere ocean warming also averages about 0.1°C over the same time period, but detailed study of the Southern Ocean has been hampered by the limited number of shipboard observations available south of 30°S (*3*–*5*). This study makes use of the large number of mid-depth temperature observations collected during the 1990s by Autonomous Lagrangian Circulation Explorer (ALACE) floats to characterize modern-day temperatures in the Southern Ocean and compares these temperature measurements with historic shipboard measurements.

ALACE floats were deployed from research ships throughout the 1990s as part of the World Ocean Circulation Experiment (WOCE). The floats sink to a predetermined pressure and follow mid-depth ocean currents for a fixed time interval of 10 to 25 days. They then rise to the surface and relay their positions and the mean temperatures recorded at depth to the Argos communications satellite system (*6*). (Newer floats also measure vertical temperature profiles as they rise to the surface; because only a fraction of the 1990s ALACE floats did this, no float profile data was included in this analysis.) A typical float provided about 50 cycles of data over 2.5 years for this study; many of the floats continue to gather data today. In the region of the world's ocean south of 30°S between 700 and 1100 m depth, 12,659 mean temperature observations were collected between 1990 and 2000 (*7*). Because the floats drift with the ocean currents, the geographic distribution of data spans the entire Southern Ocean, as indicated in Fig. 1A. ALACE observations have been used to study global and regional ocean circulation in a variety of ways (*8*–*10*), but have not previously been used to study long-term climatic variability in the ocean.

Thermistors on ALACE floats are calibrated with an accuracy of 0.001° to 0.003°C, and the sensor calibration is expected to degrade by less than 0.001°C per year. Numerical truncation required to transmit temperatures via satellite (*11*) effectively adds noise but no bias to the data, and this noise is small compared with small-scale ocean variability. Salinities were not routinely measured by ALACE floats, so compensating changes in temperature and salinity cannot be examined using these observations.

ALACE temperature observations were compared with temperature profiles collected from research ships since the 1930s. In that time period, techniques used by ships to collect ocean temperatures have evolved substantially. Before the 1970s, temperatures were derived from pressure-protected reversing thermometers, which were accurate to 0.02°C (*12*). More recent observations are from electronic conductivity-temperature-depth (CTD) and expendable bathythermograph (XBT) sensors, with accuracies of 0.001°C and 0.05°C (*13*), respectively. There are no known biases between different temperature measurement techniques. Shipboard temperatures were drawn from two separate data archives. The first, the Southern Ocean Database (SODB), includes approximately 17,724 profiles from reversing thermometer and CTD data collected between 1930 and 1990 and between 70° and 30°S (*14*). The second, the World Ocean Database 1998 (WODB), gathers a total of 35,102 Southern Ocean temperature profiles from reversing thermometer, CTD, and XBT data that extend deeper than 700 m (*15*, *16*). Both data sets are archived at standard depths, approximately every 100 m in the depth range considered here (*17*). The databases were merged, and duplicate stations that appeared in both were removed.

For this study, ALACE temperature observations were paired with geographically nearby temperature profiles. In total, 439,851 ALACE/temperature profile pairs were within 220 km of each other, and 112,103 were within 110 km. Figure 1B shows the distribution of stations used in this study as a function of decade. Temperature profile data were then linearly interpolated to match the depth of the ALACE observations. All pairs of float and hydrography point measurements

Scripps Institution of Oceanography and Department of Mechanical and Aerospace Engineering, University of California San Diego, La Jolla, CA 92093–0230, USA. E-mail: sgille@ucsd.edu